Precise and rapid detection of optical activity for accumulative femtosecond spectroscopy

Andreas Steinbacher, Johannes Buback, Patrick Nuernberger, and Tobias Brixner*

Institut für Physikalische und Theoretische Chemie, Universität Würzburg, Am Hubland, 97074 Würzburg, Germany

*brixner@phys-chemie.uni-wuerzburg.de

Abstract: We present polarimetry, *i.e.* the detection of optical rotation of light polarization, in a configuration suitable for femtosecond spectroscopy. The polarimeter is based on common-path optical heterodyne interferometry and provides fast and highly sensitive detection of rotatory power. Femtosecond pump and polarimeter probe beams are integrated into a recently developed accumulative technique that further enhances sensitivity with respect to single-pulse methods. The high speed of the polarimeter affords optical rotation detection during the pump-pulse illumination period of a few seconds. We illustrate the concept on the photodissociation of the enantiomers of methyl p-tolyl sulfoxide. The sensitivity of rotatory detection, *i.e.* the minimum rotation angle that can be measured, is determined experimentally including all noise sources to be 0.10 milli-degrees for a measurement time of only one second and an interaction length of 250 µm. The suitability of the presented setup for femtosecond studies is demonstrated in a non-resonant two-photon photodissociation experiment.

OCIS codes: (120.5410) Polarimetry; (300.6310) Spectroscopy; (320.7150) Ultrafast spectroscopy; (300.1030) Absorption.

References and links

1. C. Niezborala and F. Hache, "Measuring the dynamics of circular dichroism in a pump-probe experiment with a Babinet-Soleil compensator," J. Opt. Soc. Am. B **23**, 2418–2424 (2006).
2. L. Mangot, G. Taupier, M. Romeo, A. Boeglin, O. Cregut, and K. D. H. Dorkenoo, "Broadband transient dichroism spectroscopy in chiral molecules," Opt. Lett. **35**, 381–383 (2010).
3. I. Eom, S. Ahn, H. Rhee, and M. Cho, "Broadband near UV to visible optical activity measurement using self-heterodyned method," Opt. Express **19**, 10017–10028 (2011).
4. M. Bonmarin and J. Helbing, "Time-resolved vibrational circular dichroism and optical rotation with ultrashort laser pulses," in *Ultrafast Phenomena XVII*, M. Chergui, D. M. Jonas, E. Riedle, R. W. Schoenlein, and A. J. Taylor, eds. (Oxford University Press, 2011), 862–864.
5. P. Fischer and F. Hache, "Nonlinear optical spectroscopy of chiral molecules," Chirality **17**, 421–437 (2005).
6. J. Helbing and M. Bonmarin, "Vibrational circular dichroism signal enhancement using self-heterodyning with elliptically polarized laser pulses," J. Chem. Phys. **131**, 174507 (2009).
7. M. Bonmarin and J. Helbing, "Polarization control of ultrashort mid-IR laser pulses for transient vibrational circular dichroism measurements," Chirality **21**, E298–E306 (2009).
8. X. Xie and J. D. Simon, "Protein conformational relaxation following photodissociation of CO from carbonmonoxymyoglobin: picosecond circular dichroism and absorption studies," Biochemistry **30**, 3682–3692 (1991).
9. S. Milder, S. Bjorling, I. Kuntz, and D. Kliger, "Time-resolved circular dichroism and absorption studies of the photolysis reaction of (carbonmonoxy)myoglobin," Biophys. J. **53**, 659–664 (1988).

#163948 - $15.00 USD Received 1 Mar 2012; revised 16 Apr 2012; accepted 16 Apr 2012; published 10 May 2012

10. J. W. Lewis, R. A. Goldbeck, D. S. Kliger, X. Xie, R. C. Dunn, and J. D. Simon, "Time-resolved circular dichroism spectroscopy: experiment, theory, and applications to biological systems," J. Phys. Chem. **96**, 5243–5254 (1992).
11. A. Trifonov, I. Buchvarov, A. Lohr, F. Würthner, and T. Fiebig, "Broadband femtosecond circular dichroism spectrometer with white-light polarization control," Rev. Sci. Instrum. **81**, 043104 (2010).
12. J. Meyer-Ilse, D. Akimov, and B. Dietzek, "Ultrafast circular dichroism study of the ring opening of 7-dehydrocholesterol," J. Phys. Chem. Lett. **3**, 182–185 (2012).
13. W. Moffitt, R. B. Woodward, A. Moscowitz, W. Klyne, and C. Djerassi, "Structure and the optical rotatory dispersion of saturated ketones," J. Am. Chem. Soc. **83**, 4013–4018 (1961).
14. G. Haenisch and G. Beier, "Ein Polarimeter zur Messung schneller chemischer Reaktionen," Z. Anal. Chem. **261**, 280–286 (1972).
15. P. D. Rice, Y. Y. Shao, S. R. Erskine, T. G. Teague, and D. R. Bobbitt, "Specific rotation measurements from peak height data, with a Gaussian peak model," Talanta **36**, 473–478 (1989).
16. D. R. Bobbitt and E. S. Yeung, "Improvements in detectabilities in polarimeters using high-frequency modulation," Appl. Spectrosc. **40**, 407–410 (1986).
17. J. Lee and D. Su, "Improved common-path optical heterodyne interferometer for measuring small optical rotation angle of chiral medium," Opt. Commun. **256**, 337–341 (2005).
18. C. Feng, Y. Huang, J. Chang, M. Chang, and C. Chou, "A true phase sensitive optical heterodyne polarimeter on glucose concentration measurement," Opt. Commun. **141**, 314–321 (1997).
19. J. Lin, K. Chen, and D. Su, "Improved method for measuring small optical rotation angle of chiral medium," Opt. Commun. **238**, 113–118 (2004).
20. C. Chou, W. Kuo, T. Hsieh, and H. Teng, "A phase sensitive optical rotation measurement in a scattered chiral medium using a Zeeman laser," Opt. Commun. **230**, 259–266 (2004).
21. F. Langhojer, F. Dimler, G. Jung, and T. Brixner, "Product accumulation for ultrasensitive femtochemistry," Opt. Lett. **32**, 3346–3348 (2007).
22. F. Langhojer, F. Dimler, G. Jung, and T. Brixner, "Ultrafast photoconversion of the green fluorescent protein studied by accumulative femtosecond spectroscopy," Biophys. J. **96**, 2763–2770 (2009).
23. R. C. Jones, "A new calculus for the treatment of optical systems," J. Opt. Soc. Am. **31**, 488–493 (1941).
24. R. C. Jones, "A new calculus for the treatment of optical systems. VII. Properties of the N-Matrices," J. Opt. Soc. Am. **38**, 671–683 (1948).
25. Y. Guo and W. S. Jenks, "Photolysis of alkyl aryl sulfoxides: α-cleavage, hydrogen abstraction, and racemization," J. Org. Chem. **62**, 857–864 (1997).
26. K. Mislow, M. M. Green, P. Laur, J. T. Melillo, T. Simmons, and A. L. Ternay, "Absolute configuration and optical rotatory power of sulfoxides and sulfinate esters," J. Am. Chem. Soc. **87**, 1958–1976 (1965).
27. L. D. Barron, *Molecular Light Scattering and Optical Activity* (Cambridge Univ. Press, Cambridge, 2009).
28. D. Axelrod, D. E. Koppel, J. Schlessinger, E. Elson, and W. W. Webb, "Mobility measurement by analysis of fluorescence photobleaching recovery kinetics," Biophys. J. **16**, 1055–1069 (1976).
29. D. Lide, *CRC Handbook of Chemistry and Physics* (CRC Press, Boca Raton, 2009).
30. Stanford Research Systems, "Digital Lock-In amplifiers SR810 and SR830," Manual (1997).
31. P. Král, I. Thanopulos, M. Shapiro, and D. Cohen, "Two-step enantio-selective optical switch," Phys. Rev. Lett. **90**, 033001 (2003).
32. P. Nuernberger, G. Vogt, T. Brixner, and G. Gerber, "Femtosecond quantum control of molecular dynamics in the condensed phase," Phys. Chem. Chem. Phys. **9**, 2470–2497 (2009).
33. T. Brixner and G. Gerber, "Femtosecond polarization pulse shaping," Opt. Lett. **26**, 557–559 (2001).
34. P. Nuernberger, R. Selle, F. Langhojer, F. Dimler, S. Fechner, G. Gerber, and T. Brixner, "Polarization-shaped femtosecond laser pulses in the ultraviolet," J. Opt. A **11**, 085202 (2009).
35. Rudolph Research, "The Autopol VI Automatic Polarimeter," http://www.rudolphresearch.com (2010).

1. Introduction

Chiral molecules show optical activity, *i.e.* they rotate the polarization direction of linearly polarized light. Optical rotation is an inherently tiny effect, large optical path lengths in the range of centimeters and high concentrations are commonly employed to reach measurable optical rotation angles. Such conditions are disadvantageous for femtosecond spectroscopy, especially if one wants to apply pulse-shaping techniques, where small volumes and short path lengths are needed to achieve high intensities for nonlinear excitations and to avoid pulse distortion upon propagation through the sample. In this paper, we do not probe ultrafast chirality changes, as demonstrated (or proposed) by probing ultrafast changes in optical rotation [1–4] or circular dichroism [1–12], but we rather make use of optical rotation changes due to a stable photo-

#163948 - $15.00 USD Received 1 Mar 2012; revised 16 Apr 2012; accepted 16 Apr 2012; published 10 May 2012

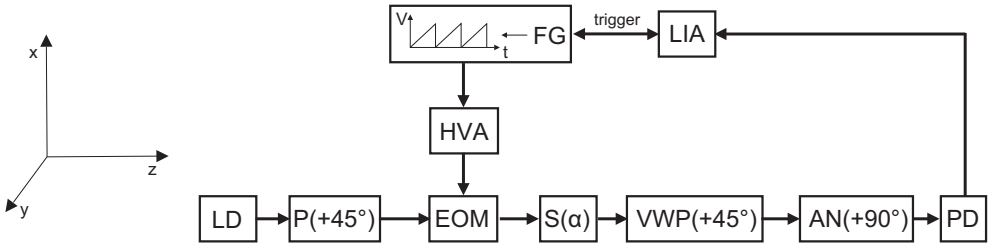

Fig. 1. Schematic diagram for the polarimeter setup. LD, laser diode; P, polarizer; EOM, electro-optic modulator; S, sample in a capillary; VWP, variable wave plate; AN, analyzer; PD, photodiode; LIA, lock-in amplifier; FG, function generator; HVA, high-voltage amplifier. Orientations are given in brackets relative to the *x* axis.

product as a probe for ultrafast dynamics initiated with femtosecond laser pulses. For an experimental implementation of this concept, we present an accumulative polarimeter setup with short path length that is fast and sensitive enough to overcome the mentioned complications.

Whereas circular dichroism is only reasonably large close to an absorption band, optical rotation is very attractive as a probe signal because it is non-zero even energetically far away from the adjacent absorption, *i.e.* the molecules can be probed without being electronically excited. It is further directly coupled to the molecular structure [13] and enantiodifferentiating in its sign. High-precision polarimeters generally do not have their focus on detection speed [14], since stationary products are observed with isotropic spatial distribution. Integration times up to minutes yield very high precision [15, 16], as used for example in high-performance liquid chromatography detectors. Polarimeters based on heterodyne detection translate the optical rotation into a phase difference, which can be detected faster. We use the heterodyne detection method of Lee and Su [17] as basis for our polarimeter since it is common-path and therefore does not require the interferometric stability of related setups [18–20]. We show the integration of the polarimeter and a probe for linear absorption spectroscopy into an accumulative scheme for femtosecond spectroscopy [21]. This affords femtosecond laser spectroscopy with rapid and precise detection of optical rotation angles as well as linear absorption. In the employed accumulative scheme, a train of femtosecond laser pulses interacts with the same sample volume such that photochemical effects are accumulated. This accumulative scheme yields higher product concentration while maintaining the femtosecond time resolution by the use of pump pulse pairs with adjustable time delay [21, 22], as is explicitly demonstrated in Section 8. The polarimeter probe utilizes the light of a continuous-wave (CW) laser diode, which is modulated by an electro-optic modulator, leading to a continuously varying polarization state. This gives the ability to transform the optical rotation of the sample into a phase difference, which can be rapidly detected by a lock-in amplifier. Adding a small phase retardation after the chiral sample leads to an effective signal amplification such that the measured phase difference then corresponds to a sensitive measurement of optical rotation.

2. Experimental setup

The principal components of our polarimeter are sketched in Fig. 1. The light of a temperature-controlled, pigtailed laser diode (LD, Thorlabs, LPS-406-FC) at 405 nm passes a thin-film polarizer (P, Codixx, colorPol UV405BC4) oriented at 45° relative to the *x* axis. An electro-optic modulator (EOM, Linos Photonics, LM0202) modulates the linearly polarized light with a sawtooth voltage (frequency: 14.5 kHz) generated by a function generator (FG, Thurlby Thandar Instr., TG4001) and amplified (40×) by a high-voltage amplifier (HVA, FLC Electronics,

#163948 - $15.00 USD Received 1 Mar 2012; revised 16 Apr 2012; accepted 16 Apr 2012; published 10 May 2012

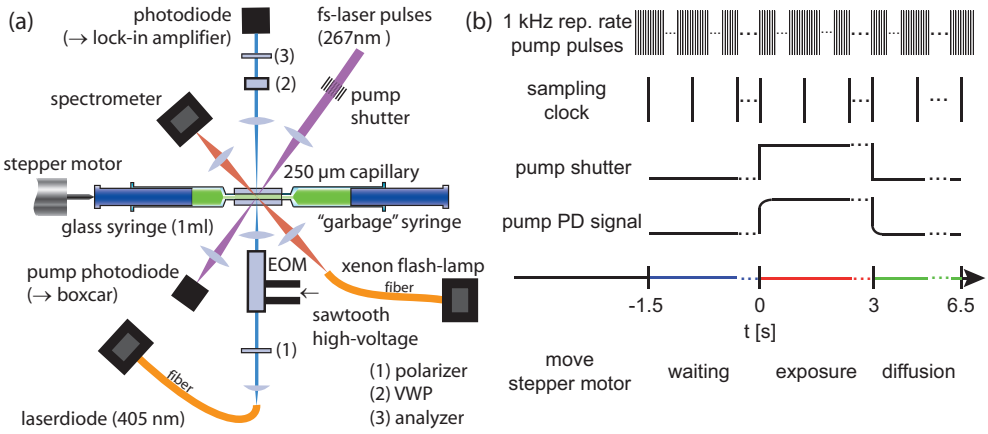

Fig. 2. (a) Schematic setup. Three beams are spatially overlapped in the capillary to record the linear absorption (red) as well as the optical rotation (blue) before, during and after illumination with femtosecond laser pulses (purple). (b) Schematic measurement procedure. Depicted is the repetition rate of the pump pulses (1 kHz), the sampling clock, the pump shutter behavior, which is equal to the detected signal of the pump photodiode (pump PD), and the time axis with dedicated time points and the measurement steps labels. The colors of the time axis correspond to those in the data of the following figures.

A400DI) to twice the half-wave voltage of the used EOM. Afterwards, the light is focused (beam diameter: 30 µm) into the sample (S) that rotates the linearly polarized light by the angle α. Then, a variable wave plate of Berek-type (VWP, New Focus, Model 5540), with its optical axis parallel to the polarizer (P), is passed before the analyzer (AN) is reached. The analyzer is a Wollaston prism (AN, Thorlabs, WP10), oriented at 45° relative to the polarizer (P), hence it is oriented parallel to the *y* axis and only one of the two output beams is analyzed. The resulting light intensity is detected with a photodiode (PD, Hamamatsu Photonics, S1337-33BQ). The phase of this signal is determined by a lock-in amplifier (LIA, Stanford Res. Sys., SR830 DSP).

The integration of this polarimeter scheme into the experimental setup for accumulative femtosecond spectroscopy is shown in Fig. 2(a). In this setup the sample is contained in a capillary (250 µm path length, cytometry cell, Hellma GmbH) shown as the central element in which three beams are spatially overlapped. The pump beam [purple beam in Fig. 2(a)] illuminates the sample with femtosecond laser pulses at 267 nm. The pump pulses are generated via third-harmonic generation of the 800 nm femtosecond laser pulses (Newport-Spectra Physics, Solstice One Box Ultrafast Amplifier) and focused weakly into the capillary resulting in a beam diameter of 200 µm. The pump beam can be blocked by the "pump shutter" before interacting with the sample volume. The time of shutter opening and closure is precisely determined relative to the lock-in amplifier data acquisition with a photodiode (pump PD, Thorlabs, DET10A/M), that detects the pump beam after passing the capillary. Furthermore, the linear absorption spectrum is obtained with very weak xenon flash-lamp pulses (Hamamatsu Photonics, L9455-11) acting as probe light [diameter: 120 µm; red beam in Fig. 2(a)]. The probe light is recorded with a spectrometer (Ocean Optics, HR2000+). The sample solution can be exchanged via a glass syringe and a stepper motor (Zaber, KT-LA28A) [21].

In the accumulative scheme the measurement procedure consists of the four steps depicted in the bottom of Fig. 2(b). In the first step, "move stepper motor" ($t < -1.5$ s), a new sample volume is pushed from the glass syringe into the capillary with the help of the stepper motor. At $t = -1.5$ s, the start of the "waiting" step (-1.5 s $< t < 0$ s), the data acquisition for the po-

#163948 - $15.00 USD Received 1 Mar 2012; revised 16 Apr 2012; accepted 16 Apr 2012; published 10 May 2012

larimeter, the linear absorption probe and the pump photodiode starts. Synchronization of these data acquisition hardwares (polarimeter: lock-in amplifier; linear absorption probe: spectrometer; pump photodiode: ADC card) is achieved by one "sampling clock" shown in the second line of Fig. 2(b). This sampling clock is simulated by a computer that generates trigger events with a given rate (we use either 50 Hz or 100 Hz in this work). Acquisition of one data set from all hardwares is triggered by one trigger event of the sampling clock.

At the start of the "exposure" step ($t = 0$ s) the pump shutter is opened. The first femtosecond pulse that hits the sample is detected by the pump photodiode as shown in the fourth line of Fig. 2(b) and that time is taken as the first "fix time point" later on. During the exposure step ($0\text{ s} < t < 3\text{ s}$) the sample is illuminated with the 1 kHz femtosecond pump pulse train shown in the top of Fig. 2(b). Closure of the pump shutter marks the start of the "diffusion" step ($t = 3$ s). Similar to the start of the exposure step the first pulse that is blocked by the pump shutter is detected by the pump photodiode and taken as the second fix time point. In the diffusion step ($3\text{ s} < t < 6.5\text{ s}$) the sample is no longer illuminated by femtosecond pump pulses and only diffusion takes place. To achieve higher resolution for the optical rotation detection as well as the linear absorption spectrum, this cycle is repeated up to five times and the single measurement curves are averaged. For this averaging, shutter timing jitter can be corrected because the two fix time points of shutter opening and closure as detected by the pump photodiode are known.

3. Polarimeter principle

The common-path optical heterodyne interferometry principle has been shown in detail by Lee and Su [17]. In contrast to their original setup, we omit the quarter-wave plate in front of the sample, since our implementation lacks a reference beam and we use the internal reference of the lock-in amplifier instead for higher precision. This leads to changes both in the relative orientations of the optical elements (Fig. 1) and in the Jones matrix calculation [23, 24]. Nevertheless, a similar sinusoidal signal can be derived, as shown below. The z axis is chosen along the propagation direction of the light and the x axis along the vertical direction (see Fig. 1). With $\mathbf{E}_{\text{in}}$ representing the linearly polarized light at 45° (due to the polarizer P in Fig. 1), $\text{EOM}(\omega t)$ representing the EOM oriented at 0° driven by a sawtooth voltage with angular frequency ω and amplitude π, $\text{S}(\alpha)$ representing the sample that rotates linearly polarized light by the angle α, $\text{VWP}(\delta, 45^\circ)$ representing the VWP with retardation δ oriented at 45° and AN representing the analyzer at 90°, the Jones vector of the light detected by the photodiode ($\mathbf{E}_{\text{out}}$) becomes:

$$\mathbf{E}_{\text{out}} = \text{AN} \cdot \text{VWP}(\delta, 45^\circ) \cdot \text{S}(\alpha) \cdot \text{EOM}(\omega t) \cdot \mathbf{E}_{\text{in}}.$$

The Jones matrix of the sample $\text{S}(\alpha)$ consists of the active 2D rotation matrix. Before and after the VWP the coordinate system is rotated by an angle $\beta = 45^\circ$ with the passive rotation matrix $\text{Rot}[\beta]$ to include the orientation of the VWP at 45° relative to the x axis. $\mathbf{E}_{\text{out}}$ then becomes

$$\begin{aligned}\mathbf{E}_{\text{out}} &= \begin{pmatrix} 0 & 0 \\ 0 & 1 \end{pmatrix} \text{Rot}[-45^\circ] \begin{pmatrix} \exp\left(\frac{i\delta}{2}\right) & 0 \\ 0 & \exp\left(\frac{-i\delta}{2}\right) \end{pmatrix} \text{Rot}[+45^\circ] \\ &\quad \times \begin{pmatrix} \cos(\alpha) & -\sin(\alpha) \\ \sin(\alpha) & \cos(\alpha) \end{pmatrix} \begin{pmatrix} \exp\left(\frac{i\omega t}{2}\right) & 0 \\ 0 & \exp\left(\frac{-i\omega t}{2}\right) \end{pmatrix} \frac{1}{\sqrt{2}} \begin{pmatrix} 1 \\ 1 \end{pmatrix}. \end{aligned} \tag{1}$$

Thus, the signal I_{out} detected by the photodiode is

$$I_{\text{out}} = |\mathbf{E}_{\text{out}}|^2 = \frac{1}{2}\left[1 + \sin(2\alpha)\cos(\delta)\cos(\omega t) + \sin(\delta)\sin(\omega t)\right], \tag{2}$$

which can be transformed into the sinusoidal form

$$I_{\text{out}} = \frac{1}{2}\left[1 + A\sin(\omega t + \phi)\right] \tag{3}$$

#163948 - $15.00 USD Received 1 Mar 2012; revised 16 Apr 2012; accepted 16 Apr 2012; published 10 May 2012

with the help of the relation

$$a\sin(\omega t)+b\cos(\omega t)=\sqrt{a^2+b^2}\sin\left[\omega t+\arctan\left(\frac{b}{a}\right)\right], \tag{4}$$

where $a=\sin(\delta)$ and $b=\sin(2\alpha)\cos(\delta)$. Thus, the amplitude A and the phase ϕ in Eq. (3) can be described through

$$A = \sqrt{a^2+b^2} = \sqrt{\sin^2(\delta)+\left[\sin(2\alpha)\cos(\delta)\right]^2}, \tag{5}$$

$$\phi = \arctan\left(\frac{b}{a}\right) = \arctan\left[\frac{\sin(2\alpha)}{\tan(\delta)}\right]. \tag{6}$$

Equation (4) is only exact if a is positive, which is true for our experiments where we use $\delta=2.3^\circ$. This value δ for the retardation setting of the VWP is found to be optimal, as shown in Section 7. The value for ϕ in Eq. (6) can then be transformed into

$$\alpha=\frac{1}{2}\arcsin\left[\tan(\delta)\tan(\phi)\right] \tag{7}$$

to reveal the optical rotation α of $S(\alpha)$ with the retardation δ known. The adjustment of the retardation setting was done experimentally by measuring the signal amplitude A [see Eq. (5)], with no sample in the capillary ($\alpha=0$), for different values for δ. Thus, we can set the value for the retardation to $\delta=(2.3\pm0.2)^\circ$. Other values are also possible if desired.

The lock-in amplifier detects the signal I_{out} in Eq. (3) for a period of time (lock-in amplifier time constant T_{LIA}) and determines the amplitude A [Eq. (5)] and the phase ϕ [Eq. (6)]. The phase is thereby relative to a reference sine oscillation. This reference can either be provided by an external signal or be internally generated. We chose the internal reference due to the higher precision of the values for A and ϕ compared to the values with external reference.

If the phase of the signal were zero for zero optical rotation, we could directly replace ϕ in Eq. (7) with the measurement value from the lock-in amplifier to obtain α. However, due to the absence of a reference beam with known absolute phase it is only possible to measure a phase change $\Delta\phi$. We define the phase change $\Delta\phi$ relative to ϕ_0, the averaged phase value measured by the lock-in amplifier during the waiting step in Fig. 2(b),

$$\Delta\phi(t)=\phi(t)-\phi_0, \tag{8}$$

with the phase value $\phi(t)$ determined by the lock-in amplifier at time t. Since we encounter only small optical rotation angles α we can apply the small-angle approximation to all terms dependent on α in Eqs. (6) and (7), with Eq. (6) then becoming $\phi\approx\frac{2}{\tan(\delta)}\alpha$. The phase change $\Delta\phi$ is then related linearly to an optical rotation change $\Delta\alpha$. For $\alpha=0.1$ deg (throughout this work all optical rotations are presented in the unit deg for degrees, or mdeg for milli-degrees, for clear presentability) the error in the phase ϕ in Eq. (6) due to the small angle approximation is 0.5 ‰ with $\delta=2.3^\circ$ as used in our experiments. We define the "angle amplification" k as

$$k=\frac{2}{\tan(\delta)}, \tag{9}$$

which describes the factor between the optical rotation α and the phase ϕ detected by the lock-in amplifier. Equation (7) then becomes $\alpha k\approx\phi$.

Considering now that we measure a phase difference $\Delta\phi$ we exploit this linear relationship of ϕ with α to obtain an optical rotation change $\Delta\alpha$. With a phase ϕ_0 corresponding to a known optical rotation α_0, e.g. the phase difference for the achiral solvent corresponding to $\alpha_0=0$ deg, one can directly calculate the absolute optical rotation to $\alpha=\alpha_0+\Delta\alpha$.

#163948 - $15.00 USD Received 1 Mar 2012; revised 16 Apr 2012; accepted 16 Apr 2012; published 10 May 2012

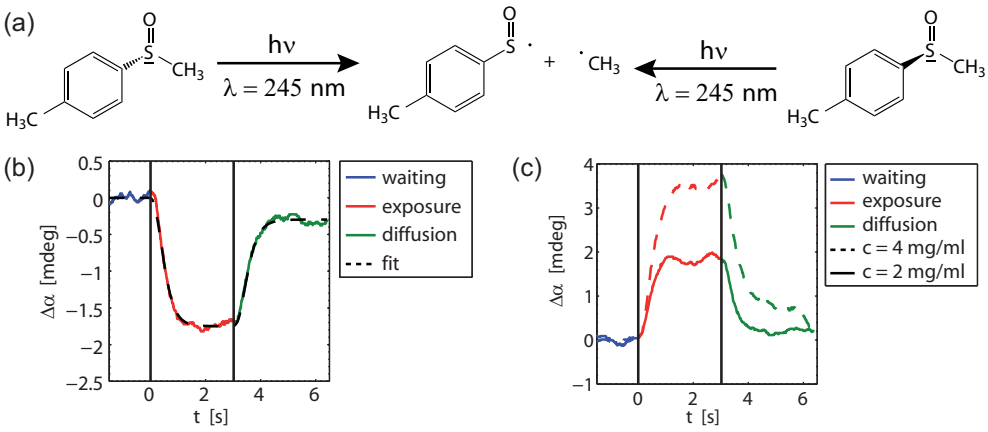

Fig. 3. (a) Photodissociation of methyl p-tolyl sulfoxide molecules in the case of the R- (left) and S-enantiomer (right). After irradiation with UV light, the sulfoxide molecules break at the stereogenic center, resulting in two achiral products (middle) [25]. (b) Optical rotation measurement for the R-enantiomer in acetonitrile with a concentration of $c =$ 2 mg/ml, a sampling rate of 100 Hz and a lock-in amplifier time constant of $T_{\mathrm{LIA}} = 100$ ms. The data are plotted in blue, red, and green corresponding to the colors of the time intervals introduced in Fig. 2(b). The two vertical black lines indicate the time window during which the pump shutter is open. A fit (black dashed line), with the model introduced in Section 5 (or more detailed in Appendix A), is presented. (c) Optical rotation measurements for the S-enantiomer in acetonitrile with concentrations of $c = 4$ mg/ml (dashed) and $c = 2$ mg/ml (solid), a sampling rate of 100 Hz and a lock-in amplifier time constant of $T_{\mathrm{LIA}} = 100$ ms.

4. Exemplary data

We use the photoreaction presented in Fig. 3(a) to test our polarimeter. Irradiation of methyl p-tolyl sulfoxide with UV light leads to bond cleavage at the stereogenic center (the sulfur atom) and therefore to two non-chiral products [25]. Thus, the absolute magnitude of the rotation angle of the solution decreases when starting with either of the two enantiomers. We probe the optical rotation of R-(+)-methyl p-tolyl sulfoxide with the setup of Fig. 2(a) and obtain the typical data shown in Fig. 3(b). During the waiting step (blue), *i.e.* before illumination, a constant signal is acquired, referring to zero optical rotation change. At $t = 0$ [left vertical line in Fig. 3(b)] the pump shutter opens and the illumination with 267 nm femtosecond laser pulses starts. During this exposure step (red) the optical rotation decreases rapidly due to the photodecomposition of the chiral reactant taking place. After the end of illumination [the pump shutter is closed at the right vertical line in Fig. 3(b)], *i.e.* during the diffusion step (green), reactant molecules diffuse into the probe volume, and product molecules diffuse out of the probe volume. This process increases the optical rotation angle again. Note that the diffusion effect persists as well in the red part of the curve while the pump shutter is open. Hence, the final value of the exposure step ($t = 3$ s) refers to an equilibrium between the diffusion and the destruction of reactant molecules by the femtosecond laser pulses. The value at the end of the diffusion step ($t = 6.5$ s) would be close to the initial optical rotation value due to diffusion, if the waiting time after illumination were long enough and if the pump volume were in contact with an infinite reservoir of the intact reactant.

Literature values for the specific rotation of the molecule in question [13] state a positive optical rotation angle for the R-enantiomer. Photodestruction of the R-enantiomer therefore should lead to a decrease in optical rotation, and this is indeed what we observe in Fig. 3(b).

#163948 - $15.00 USD Received 1 Mar 2012; revised 16 Apr 2012; accepted 16 Apr 2012; published 10 May 2012

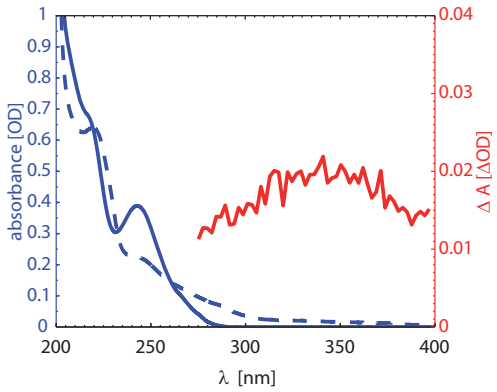

Fig. 4. Linear absorption spectra of methyl p-tolyl sulfoxide before (blue solid line) and after illumination (blue dashed line) with a concentration of $c = 0.015$ mg/ml and acetonitrile as solvent. The linear absorption spectrum for the used sulfoxide molecules shows an absorption band at $\lambda_{\max} = 245$ nm, whereas for small wavelengths the influence of the solvent is dominant. After UV irradiation, the sulfoxide molecules break at the stereogenic center, resulting in two non-chiral fragment products, as shown in Fig. 3(a). These products lead to a non-zero absorption in the region around 325 nm (blue dashed curve). The red curve shows the linear absorption change of an accumulative femtosecond experiment with the R-enantiomer and $c = 2$ mg/ml in acetonitrile at a sampling rate of 50 Hz.

For comparison, we also recorded the optical rotation change starting with the other enantiomer, S-(-)-methyl p-tolyl sulfoxide, and obtain the data shown in Fig. 3(c) for two different concentrations $c = 2$ and 4 mg/ml. As expected, the optical rotation change is of opposite sign.

Having confirmed qualitatively that the polarimeter setup can be used to measure optical rotation changes, we now discuss how to extract rotation angles quantitatively. For this purpose, we determine the expected optical rotation for this molecules and our setup conditions from literature values. The extrapolation of the literature value $[\alpha]_{589\ \mathrm{nm}}^{20^\circ\mathrm{C}} = \pm 145$ deg [26] for the specific optical rotation was done with the Drude equation [27]. By extrapolation to the resonance at $\lambda = 245$ nm (see Fig. 4), a specific rotation at $\lambda = 405$ nm, which is the wavelength used in the polarimeter, of $[\alpha]_{405\ \mathrm{nm}}^{20^\circ\mathrm{C}} = \pm 400$ deg is obtained. Note that the sign depends on the enantiomer and is positive for the R-form and negative for the S-form. Thus, we can calculate the optical rotation α_0 of our sample with the path length $d = 250$ µm and concentration $c = 1$ mg/ml to be $\alpha_0 = \pm 1.0$ mdeg. Since the literature value corresponds to a solution in acetone, we measured the optical rotation also with a commercial polarimeter (JASCO Circular Dichroism Spectropolarimeter J-815) in acetonitrile (the solvent used for the data in Fig. 3) supporting the extrapolation with the Drude equation with an optical rotation angle of ± 1.0 mdeg for the same conditions ($c = 1$ mg/ml and $d = 250$ µm).

If all chiral molecules within the pump volume are destroyed by the femtosecond pulse train in the experiment of Fig. 3(a), an optical rotation change of $\Delta\alpha = -2.0$ mdeg is expected for a concentration of $c = 2$ mg/ml, which is twice as high as in the steady-state measurement ($c = 1$ mg/ml). Instead, the observed value for $\Delta\alpha \approx -1.7$ mdeg is slightly lower [Fig. 3(a)]. Similarly, for the S-enantiomer [Fig. 3(b)] we observe at the concentrations $c = 2$ and 4 mg/ml maximal optical rotation changes of $\Delta\alpha \approx +1.8$ and $+3.8$ mdeg, respectively, again nearly corresponding to the expectations from steady-state optical rotation. The fact that we do not observe exactly the expected $\Delta\alpha$ values is explicable by diffusion due to which not all molecules are destroyed, but an equilibrium between diffusion and destruction evolves. Quantitative treatment of this effect will be provided in Section 5 or more detailed in Appendix A. We can

#163948 - $15.00 USD Received 1 Mar 2012; revised 16 Apr 2012; accepted 16 Apr 2012; published 10 May 2012

therefore conclude that the presented polarimeter can accurately measure optical rotation.

Besides the optical rotation data we also collect linear absorption spectra of the molecules in the spectral range from 275 to 400 nm. We calculate the absorbance change $\Delta A(\lambda)$, exemplarily shown in Fig. 4 as a red line, as $\Delta A = \log_{10}(I_0/I)$, with I being the averaged intensity from $t = 2.9$ s to $t = 3$ s and I_0 being the averaged intensity from $t = -0.1$ s to $t = 0$ s.

To confirm the results of the linear absorption measurement we illuminated a sample solution (5 mm thickness) with a UV lamp for approximately one hour and collected the absorption spectra before and after illumination with a UV-VIS spectrometer (Hitachi, U-2000). The blue solid line in Fig. 4 shows the absorption spectra before illumination, whereas the blue dashed curve shows the linear absorption spectra after illumination. The photoreaction leads to a non-zero absorption in the region above 300 nm, which is also present in the result of our measurements in the accumulative setup (red curve in Fig. 4).

After the bond cleavage, the products may further undergo secondary reaction steps. Since we do not know these reactions and their characteristic time scales, a quantitative comparison of the ΔA value measured within a few seconds and the changes in the linear absorption spectrum after one hour of illumination is not appropriate. Nevertheless, we can conclude from these data that a reaction destroying the chiral molecules has taken place in both cases, *i.e.* under steady-state conditions and under accumulative conditions. The latter is directly confirmed by the linear absorption probe measurement. However, since linear absorption is not enantiodifferentiating, the further discussion will concentrate on the polarimeter probe measurements.

5. Data modeling

The effect of diffusion into and out of the probing volume needs to be considered to understand the data shown in Fig. 3, especially if one wants to extract quantitative information about the time evolution of the concentrations of the involved chemical species. Since an analysis by applying the full diffusion equation [28] would be complex, we simplify the modeling by using effective exchange rates between the different irradiated sample volumes [21, 22]. Thus, we call "pump volume" the sample volume irradiated with the femtosecond laser pulses, while the "probe volume" corresponds to the sample volume that is probed with the 405 nm polarimeter beam. The diffusion rate between these volumes is described by d_{pr}, whereas d_{pu} refers to the diffusion rate between the pump volume and the surrounding solution. Furthermore, the photoconversion rate, *i.e.* the change in optical rotation per unit time, is described by η. A more elaborate definition and derivation of the model is presented in Appendix A, which additionally comprises the instrument response function of the lock-in amplifier.

As an example for the applicability of this fitting model, the experimental data for the R-enantiomer ($c = 2$ mg/ml) in Fig. 3(b) was fitted (black dashed curve) resulting in the following values: $\alpha_0 = 2.13$ mdeg, $\eta = 2.39 \times 10^{-3}$/pulse, $d_{\mathrm{pu}} = 3.58\ \mathrm{s}^{-1}$, and $d_{\mathrm{pr}} = 4.69\ \mathrm{s}^{-1}$. The agreement of the fit with the experimental data is excellent, which justifies the simplified treatment of the diffusion modeling. The deviation of α_0 with respect to the expected value 2.0 mdeg might originate from the retardation setting δ, which is not known exactly, and hence might cause a small deviation (see Section 3). The interpretation of the absolute values of d_{pu} and d_{pr} is not meaningful since they are alignment dependent. However, since our main goal is the obtention of η and α_0, the determination of the diffusion rates is necessary. Furthermore, relative values can provide some information about the photochemistry taking place (see Section 6.2).

6. Results

In the following, two applications serve as illustrations of the polarimeter and data model. First we investigate the photoconversion efficiency η by varying the excitation pulse energy and second, we study the influence of the diffusion rates d_{pu} and d_{pr} by varying the solvent.

#163948 - $15.00 USD Received 1 Mar 2012; revised 16 Apr 2012; accepted 16 Apr 2012; published 10 May 2012

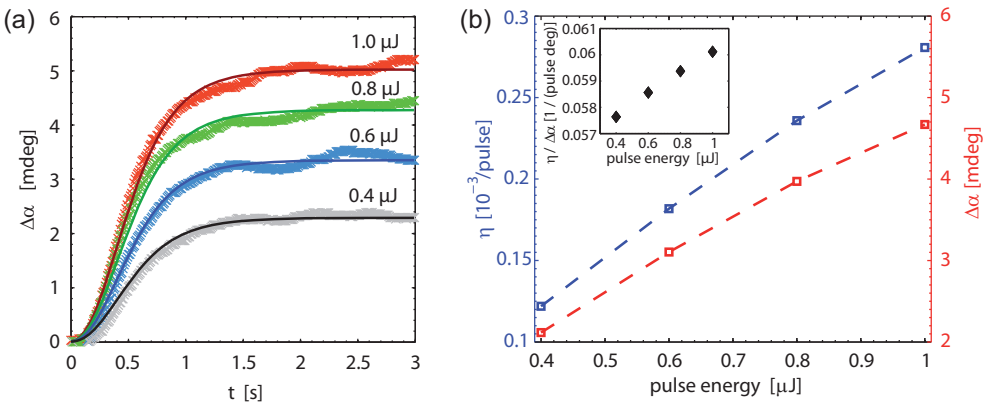

Fig. 5. (a) Fitting result (solid curves) [Eq. (15)] and experimental data (crosses), recorded with 100 Hz, of the exposure part. The global fit results in a linear relationship of η and the pump power [see (b)]. With a concentration of $c = 6$ mg/ml of S-(-)-methyl p-tolyl sulfoxide in acetonitrile, the expected optical rotation $\Delta\alpha$ change of ≈ 5.0 mdeg is achieved only in the case of 1.0 µJ. In the case of lower intensities an equilibrium at smaller optical rotations is obtained. (b) Dependence of the fit parameter η on the pulse energy as given by the global fit to the experimental data in (a) (blue), and dependence of the optical rotation change $\Delta\alpha$ on the pulse energy (red). To corroborate that the two graphs do not form two straight lines, their ratio is shown as an inset (note the scale).

6.1. *Pulse energy variation*

We use a solution of S-(-)-methyl p-tolyl sulfoxide molecules in acetonitrile with a concentration of $c = 6$ mg/ml. This solution is irradiated with pulse energies from 0.4 to 1.0 µJ and the change in optical rotation is monitored as a function of time during exposure [Fig. 5(a)]. Since we look at the S-enantiomer, the optical rotation change is positive during illumination. For the highest pulse energy, the observed optical rotation change is close to the theoretical maximum optical rotation change of 6.0 mdeg. In the case of lower pulse energies the equilibrium is reached at smaller optical rotations. The parameters of the model [Appendix, Eq. (15)] are obtained via global fitting to all experimental data sets of Fig. 5(a). This results in only one value for $\alpha_0 = 6.09$ mdeg and $d_{\mathrm{pu}} = 3.09\ \mathrm{s}^{-1}$ for all curves, since nothing except the pulse energy was changed. Hence, only the parameter η is allowed to vary between the different curves in Fig. 5(a), but still the experimental data is described well with the model.

The obtained conversion efficiencies are presented in Fig. 5(b) (blue) and reveal a nearly perfect linear relationship with the pulse energy. Furthermore, in Fig. 5(b) (red) the reached optical rotation change $\Delta\alpha$ for each pulse energy is presented. For increasing pulse energies, the optical rotation change $\Delta\alpha$ increases slower than the value for the photoconversion efficiency η. Hence, for even higher pulse energies the value for $\Delta\alpha$ will saturate, while the value for η should still increase linearly. Note that the pump diameter is 200 µm making multiphoton process contributions unlikely. This non-linear rise of $\Delta\alpha$ with the pulse energy meets the expectation, since at a given pulse energy all molecules in the probe volume are destroyed, limiting the optical rotation change $\Delta\alpha$ to a maximum value, whereas η in a good approximation scales linearly with the pulse energy.

6.2. *Solvent variation*

To study the impact of solvent viscosity, we compare acetonitrile and isopropanol as solvents for the R-enantiomer with a concentration of $c = 2$ mg/ml at a pulse energy of 0.8 µJ. Thus,

#163948 - $15.00 USD Received 1 Mar 2012; revised 16 Apr 2012; accepted 16 Apr 2012; published 10 May 2012

Table 1. Dependence of the Diffusion Rates d_{pu} and d_{pr} on the Solvent

solvent	d_{pu} $\left[\mathrm{s}^{-1}\right]$	d_{pr} $\left[\mathrm{s}^{-1}\right]$
acetonitrile	3.5739	4.4795
isopropanol	1.9789	1.8191

except for the solvent, all other experimental parameters are identical. The results for the diffusion rates of the fits are listed in Table 1. The diffusion rates of acetonitrile are larger than those of isopropanol, which is a direct consequence of acetonitrile having a smaller viscosity ($\eta_v = 0.369$ mPa s) than isopropanol ($\eta_v = 2.038$ mPa s) [29]. This result does not only show the applicability of the derived model, but also that the right calibration, *i.e.* the determination of the diffusion rates, is crucial to extract quantitative information from accumulative femtosecond spectroscopy experiments. Note, although not differing drastically, that these values cannot be compared directly to the values obtained in Section 6.1 because a different concentration was employed and the spatial overlap of the pump and the polarimeter beam (see Fig. 2) was slightly moved. The calibration process should thus be carried out for each arrangement such that the desired photoconversion efficiency can always be extracted from the experiment.

7. Rotation-angle resolution

Two decisive characteristics of the polarimeter are rotatory resolution and acquisition time. The theoretical limit in the time domain is set by the time constant of the lock-in amplifier, since one has to wait approximately three to five times the time constant to reveal a reliable phase value (see Appendix) [30]. The resolution in optical rotation is more complicated to determine. Theoretically, it is given by the angular phase resolution of the lock-in amplifier, in our case 8 mdeg [30], which would lead to a resolution of the optical rotation of 0.16 mdeg for a retardation setting of $\delta = 2.3^\circ$ (which will be shown to be optimal below). Lee and Su have calculated a theoretical limit of 0.035 mdeg [17] considering besides the angular resolution of the lock-in amplifier also the second-harmonic error and the polarization-mixing error. However, this value is not reached in an actual experiment due to electronic noise, scattering in the sample solution or intensity fluctuations of the laser diode, to mention just a few effects. Thus, we decided to determine the true resolution of the polarimeter experimentally rather than theoretically. For this purpose, we fill the capillary with solvent only (acetonitrile) and repeat the measurement procedure of Section 4, thus including all noise effects. The data should be basically a horizontal line as no change in rotation angle should occur upon irradiation with the femtosecond pulse train. The recorded fluctuations due to noise are assumed to be Gaussian distributed, which was confirmed by statistical analysis of the distribution of the data points. A step change in such data can be resolved if it is greater than two times the standard deviation of the noise. Hence, we calculate the standard deviation of the solvent data and multiply the result by two to obtain the rotatory resolution of the polarimeter.

The result of this noise analysis can be seen in Fig. 6 for different settings of the retardation δ of the VWP and different time constants of the lock-in amplifier T_{LIA}. The resolution gets better with longer time constants. Concerning the retardation δ of the variable wave plate, a setting of $\delta = 2.3^\circ$ is best for our purposes, revealing an optimal resolution of 0.10 mdeg within only 1 s of measuring time ($T_{\mathrm{LIA}} = 100$ ms). This value of 0.10 mdeg is smaller than the value of 0.16 mdeg determined by the resolution of the lock-in amplifier because of data averaging. On the other hand it is somewhat larger than the purely theoretical value of 0.035 mdeg by Lee and Su [17] because we include all experimental noise sources.

#163948 - $15.00 USD Received 1 Mar 2012; revised 16 Apr 2012; accepted 16 Apr 2012; published 10 May 2012

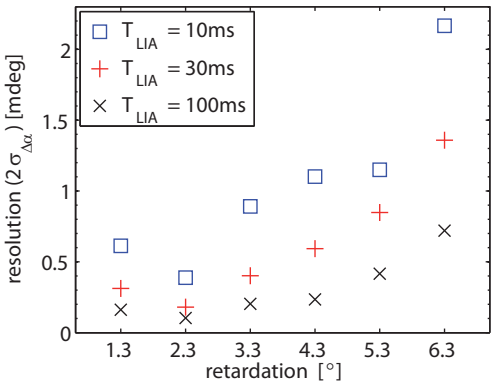

Fig. 6. Resolution of the optical rotation change $\Delta\alpha$ (at 1 s measurement time) for different settings of the retardation δ [Eq. (7)] and different time constants of the lock-in amplifier. The resolution has its optimum at a retardation of $\delta = 2.3^\circ$ for all time constants. The best resolution value, at a time constant of 100 ms, is 0.10 mdeg.

Theoretically, the angle amplification k should get infinitesimally large when approaching a retardation setting of $\delta = 0^\circ$ according to Eq. (9), which should result in an infinitesimally small resolution. However, the amplitude A of the modulation given [Eq. (5)] for such small retardations would be very small (zero in the case of $\delta = 0^\circ$). Since the lock-in amplifier reveals a higher noise level for smaller signal amplitudes the effect of the optimal retardation setting should feature a local minimum. Figure 6 shows that the resolution for a retardation value of $\delta = 1.3^\circ$ is worse than for $\delta = 2.3^\circ$, which is a direct consequence from this relationship.

If one calculates the change in optical rotation per laser pulse, which is essentially the fitting parameter η (see Appendix A), we obtain a resolution on the order of 10^{-4} mdeg (see Fig. 5). In ultrafast time-resolved pump-probe experiments [1], a resolution on the order of 10^{-1} mdeg has been demonstrated. However, the technique employed there differs significantly from our approach, whose sensitivity is due to the accumulation of products over many laser pulses, but does not measure time-resolved chirality changes on an ultrafast time scale.

8. Femtosecond time resolution

As mentioned before, the accumulative spectroscopy technique allows a femtosecond time resolution by using a pair of pump pulses [21,22] which are delayed with respect to each other. To verify this also for the optical rotation detection of the present work, we determine the maximum time resolution achievable with the employed laser system by initiating the photoreaction of Fig. 3(a) via a non-resonant absorption of two photons of different color. The optical rotation signal as a function of the time delay within the pump pulse pair reflects the time resolution of the setup and ideally would follow the cross-correlation of the pump pulse pair.

To generate a pair of pump pulses with different central frequencies, a fraction of the 800 nm laser output is frequency-doubled in a β-barium borate crystal (BBO, thickness 200 µm, cut at 29.2°), yielding 400 nm pulses. The fundamental and frequency-doubled beams are separated in a Mach-Zehnder-type setup [Fig. 7(a)]. While the 400 nm beam path is kept fixed, the delay $\Delta\tau$ is introduced via a computer-controlled linear stage which de- or increases the length of the beam path of the 800 nm beam. A half-wave plate is included in the 400 nm beam to achieve parallel polarizations. The beams can be attenuated separately with the help of two neutral density filter wheels [see Fig. 7(a)] and are finally weakly focused into the capillary at a diameter of ≈ 250 µm. For the 400 nm beam we use a pulse energy of 5 µJ while the 800 nm

#163948 - $15.00 USD Received 1 Mar 2012; revised 16 Apr 2012; accepted 16 Apr 2012; published 10 May 2012

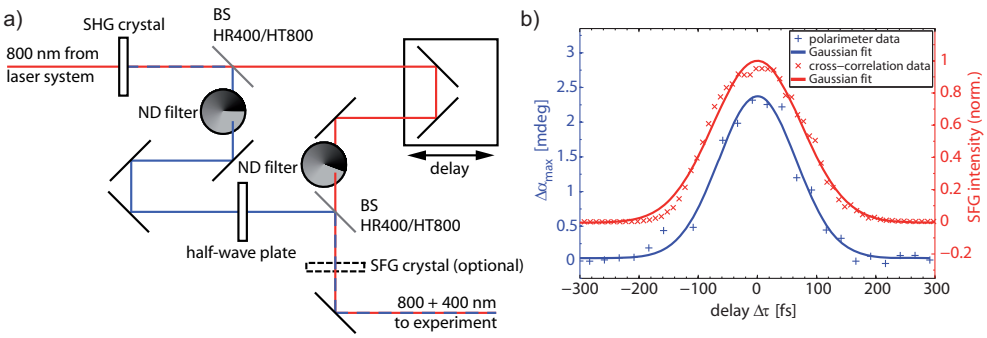

Fig. 7. (a) Sketch of the setup used to introduce the time delay between the pump pulse pair. For the measurement of the cross-correlation a SFG crystal is included after the second dichroic mirror. (b) Comparison of the cross-correlation and the polarimeter measurement with two pump pulses. The shape of both curves are nearly identical, as can be seen from the two Gaussian fits. The data are vertically offset for clarity; note the different ordinates.

beam is adjusted to 4 μJ, so that the photoreaction does not occur measurably via multiphoton absorption from either only the 400 nm or the 800 nm pulses. The measurement is identical to the description in Section 2 except that instead of a train of pulses we now use a train of pulse pairs. Thus, a measurement curve analogous to Fig. 3 is recorded for every time delay $\Delta\tau$ of the pump pulse pair. The maximum optical rotation change, *i.e.* the averaged optical rotation change for 2.5 s $\leq t \leq$ 3.0 s, is then plotted as a function of $\Delta\tau$.

The result of an experiment with the S-enantiomer ($c = 5$ mg/ml, $T_{\mathrm{LIA}} = 100$ ms, sampling rate 100 Hz) is shown in Fig. 7(b) (blue plus signs). A strong change in optical rotation is evident if the pulses of the pump pulse pair overlap temporally. To determine $\Delta\tau = 0$ and to record the cross-correlation [red crosses in Fig. 7(b)] we use another BBO crystal (100 μm, 44.3°) for sum frequency generation (SFG) at 267 nm which is detected by a photodiode after blocking the 400 and 800 nm beam with a filter (Schott UG11).

The polarimeter data as well as the cross-correlation data were fitted with a Gaussian function and juxtaposed in Fig. 7(b), disclosing their identical temporal behavior. Hence, the time resolution of the accumulative polarimeter setup is indeed predominantly limited by the femtosecond pulse duration. We want to emphasize that we do not detect an ultrafast change in optical rotation, but a change in optical rotation between reactants and stable products is probed by a CW light source. Nevertheless, femtosecond time resolution for monitoring the chemical reaction dynamics is achieved by using a pair of pump pulses with adjustable delay. The setup is hence applicable to determine the ultrafast dynamics of a chiral system undergoing a change in optical activity after the (resonant) interaction with two femtosecond pulses.

As an outlook, imagine a racemic solution illuminated with specific pulsed laser fields so that the interconversion of the enantiomers is asymmetric (*e.g.*, a scenario as in [31]). While standard absorption measurements cannot reveal this, our accumulative polarimeter is a sensitive device which should be able to detect such a photoderacemization, and it is fast enough so that the search for the adequate electric fields can be done in a closed-loop procedure based on a genetic algorithm [32]. Such an approach might further benefit from shaped femtosecond pulses whose polarization state can be adjusted in a well-defined way [33], even in the ultraviolet [34].

9. Conclusion

Within this work, we presented a setup combining common-path optical heterodyne interferometry and an accumulative technique for femtosecond laser spectroscopy to measure small

#163948 - $15.00 USD Received 1 Mar 2012; revised 16 Apr 2012; accepted 16 Apr 2012; published 10 May 2012

changes in optical rotatory power. The functionality of the technique was demonstrated for a photoreaction of chiral sulfoxides and simultaneously recorded linear absorption spectra. Optical rotation is an attractive signal for monitoring chemical reactions involving enantiomers. The presented setup has an experimentally determined angular resolution of 0.10 mdeg including all noise sources, which is better than most commercial devices. However, here we need a measurement time of only one second, an interaction length of only 250 µm and a probe beam size (aperture) of only 30 µm for the polarimeter, in contrast to commercially available polarimeters [35] (interaction length: on the order of centimeters; aperture: > 1 mm; measurement time: ≈ 10 s). In addition, it is possible to gain femtosecond time resolution by utilizing a pair of pump pulses. In this way, the ultrafast dynamics of a photoreaction can be revealed if a stable photoproduct with a different optical activity than the reactant is formed after the interaction with two femtosecond laser pulses with proper temporal delay, phase, and polarization.

Appendix A: Determination of sample and instrument response

In this appendix, we want to derive the model which led to the fit function used in the main body of the paper. As mentioned in Section 5, it is important to take diffusion effects into account to be able to model the acquired data of the polarimeter correctly. Thus, in a first step we describe the response of the sample by a simple diffusion model. In a second step, we elucidate the response function of the used lock-in amplifier. Afterwards, these two functions are combined, resulting in the final fitting model used to describe the measured data.

Sample response

For better visualization of the used variables, the definition of the effective volumes is sketched in the inset of Fig. 8. We call "pump volume" (blue disk in Fig. 8) the sample volume that is irradiated with the femtosecond laser pulses, which creates an optical rotation labeled α_{pu}. The sample volume that is probed with the 405 nm polarimeter beam, called "probe volume" (yellow disk in Fig. 8), exhibits an optical rotation α_{pr}. Before the sample is irradiated ($t < 0$),

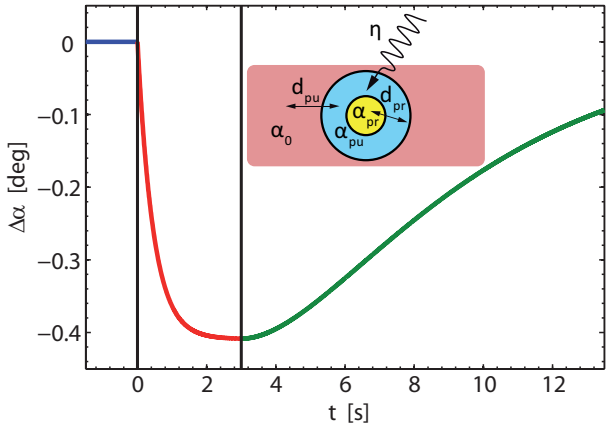

Fig. 8. Simulated example for the diffusion model obtained via Eq. (12) and the condition $\Delta\alpha = \alpha_{\mathrm{pr}} - \alpha_0$ with the following parameters: $\alpha_0 = 0.5$ deg, $\eta = 1.8 \times 10^{-3}$ / pulse, $d_{\mathrm{pr}} = 0.2\ \mathrm{s}^{-1}$, $d_{\mathrm{pu}} = 0.4\ \mathrm{s}^{-1}$, $\tau = 3.0$ s. The curve shows the decay due to illumination (red) and the following increase in optical rotation due to diffusion effects (green). Inset: optical rotations α_i in different volumes i defined by the beam geometry with rates for diffusion d_{i} and photoconversion efficiency η.

#163948 - $15.00 USD Received 1 Mar 2012; revised 16 Apr 2012; accepted 16 Apr 2012; published 10 May 2012

the optical rotation in the whole capillary is constant and equal to α_0, $\alpha_{pu}(0) = \alpha_{pr}(0) = \alpha_0$. At $t = 0$ the exposure with femtosecond laser pulses starts and lasts for the time τ, which is equal to 3.0 s in our case. During this irradiation ($0 \leq t \leq \tau$) the concentration of the pump volume changes according to [21]

$$\frac{d\alpha_{pu}(t)}{dt} = d_{pu}[\alpha_0 - \alpha_{pu}(t)] - \eta\,\alpha_{pu}(t), \qquad \alpha_{pr}(t) \equiv \alpha_{pu}(t), \tag{10}$$

with d_{pu} being the diffusion rate between the pump and the surrounding solution (see Fig. 8) and η is the photoconversion rate, *i.e.* the change in optical rotation per unit time. In the following, the photoconversion rates are given in the unit $[1/\text{pulse}]$, which can be calculated by dividing η with the repetition rate (1 kHz) of the femtosecond laser system. During the illumination period the probe volume is approximately described by the same time evolution as the pump volume. After the exposure time ($t > \tau$) only diffusion persists, which is described through

$$\frac{d\alpha_{pu}(t)}{dt} = d_{pu}[\alpha_0 - \alpha_{pu}(t)], \qquad \frac{d\alpha_{pr}(t)}{dt} = d_{pr}[\alpha_{pu}(t) - \alpha_{pr}(t)], \tag{11}$$

where d_{pr} is the diffusion rate between the pump and probe volume (see Fig. 8). The complete solution of the systems of differential equations [Eqs. (10) and (11)] is

$$\alpha_{pr}(t,\tau) = \alpha_0 \times \begin{cases} 1 & t < 0 \\ \frac{d_{pu}+\eta\exp[-(d_{pu}+\eta)t]}{d_{pu}+\eta} & 0 \leq t \leq \tau \\ \frac{d_{pu}\exp[d_{pr}(\tau-t)-(d_{pu}+\eta)\tau]\{-1+\exp[(d_{pu}+\eta)\tau]\}\eta - d_{pu}(d_{pu}+\eta)}{(d_{pr}-d_{pu})(d_{pu}+\eta)} & \\ + \frac{d_{pr}\left(d_{pu}+\{1-\exp[d_{pu}(\tau-t)]+\exp(-d_{pu}t-\eta\tau)\}\eta\right)}{(d_{pr}-d_{pu})(d_{pu}+\eta)} & t > \tau \end{cases}. \tag{12}$$

In order to exemplify Eq. (12) we show in Fig. 8 the temporal evolution of optical rotation for one particular set of constants. The initial decay starts at $t = 0$ s due to illumination and is then limited via the diffusion rate d_{pr}. After the illumination ($t \geq 3.0$ s), only diffusion driven by both diffusion rates persists, which leads to a re-increase in optical rotation.

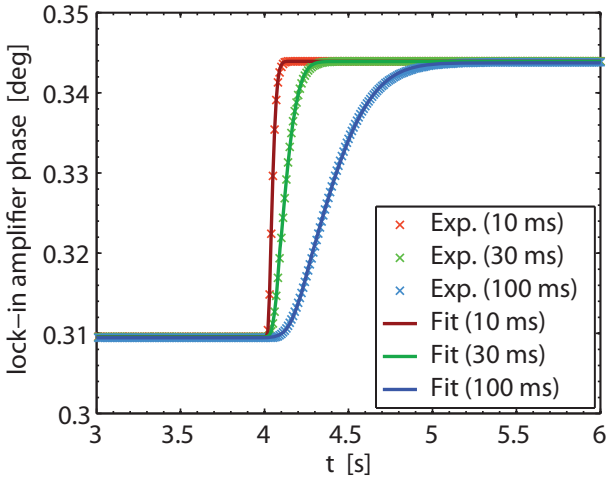

Fig. 9. Response function of the used lock-in amplifier. The experimental data, sampled at 100 Hz, is shown in crosses for different lock-in amplifier time constants (red: 10 ms, green: 30 ms, blue: 100 ms). Equation (14) was used for the fitting procedure (solid lines) resulting in the values presented in Table 2.

#163948 - $15.00 USD Received 1 Mar 2012; revised 16 Apr 2012; accepted 16 Apr 2012; published 10 May 2012

Table 2. Results of the Fitting Procedure of the Response of the Lock-In Amplifier Presented in Fig. 9*

LIA time constant T_{LIA} [s]	0.010	0.030	0.100	relation with T_{LIA}
delay m [s]	0.0325	0.0801	0.2480	$\approx 2.4\ T_{\mathrm{LIA}} + 0.0084$ s
variance b_1 [s]	0.0075	0.0238	0.0805	$\approx 0.8\ T_{\mathrm{LIA}}$
variance b_2 [s]	0.0280	0.0842	0.2776	$\approx 2.8\ T_{\mathrm{LIA}}$

*The fit reveals a linear relationship for all parameters m, b_1, and b_2, with respect to the lock-in-amplifier time constant T_{LIA} as indicated by the equations in the last column.

Instrument response

In addition to this sample response we have to consider the instrument response function of the lock-in amplifier for accurate modeling of the experimental data. We measured the response of the lock-in amplifier by generating a sinusoidal signal which changes its phase and amplitude abruptly at a given time point ($t = 4.0$ s, see Fig. 9) and measure how fast the new phase value is detectable at the output (Fig. 9). Note that Fig. 9 shows rather the convolution of the response function with a step function than the response function itself. In the case of an infinitely fast response a step function would be observed. By contrast, we observe a delayed and smoothed rise for different lock-in amplifier time constants, as expected. We assume the response function $R_{\mathrm{LIA}}(t)$ to be an asymmetric Gaussian, consisting of two moieties with different widths

$$R_{\mathrm{LIA}}(t) = \frac{2A}{\sqrt{2\pi}(b_1+b_2)} \left\{ \Theta(m-t) \exp\left[-\frac{(t-m)^2}{2b_1^2} \right] + \Theta(t-m) \exp\left[-\frac{(t-m)^2}{2b_2^2} \right] \right\}. \quad (13)$$

Here A represents the area under the curve of the asymmetric Gaussian-shaped function $R_{\mathrm{LIA}}(t)$, the b_i^2 indicate the Gaussian variances for each side, m is the position of the maximum of R_{LIA} and Θ is the Heaviside step function. The convolution of the asymmetric Gaussian $R_{\mathrm{LIA}}(t)$ in Eq. (13) with a step function is given by the integration

$$\mathrm{Erf}_{\mathrm{LIA}}(t) = \frac{2}{\sqrt{\pi}} \int_{-\infty}^{t} R_{\mathrm{LIA}}(x)\mathrm{d}x + O \quad (14)$$

with O being a phase offset. Equation (14) corresponds directly to the data in Fig. 9. The best fits of Eq. (14) to the experimental data (crosses) for three different time constants of the lock-in amplifier are shown as solid lines in Fig. 9. The obtained fit parameters are listed in Table 2. As can be seen from the linear relationship of the fit parameters (last column in Table 2) with respect to the time constant T_{LIA} and the good agreement of the fits with the experimental data in Fig. 9, the model [Eq. (13)] for the response function is satisfactory. The linear relationship is comprehensible since in case the time window length for integration (*i.e.*, the lock-in amplifier time constant T_{LIA}) is larger, the final values for the amplitude and phase are reached more slowly. The parameters b_1 and b_2 describe the width of the response function linearly, therefore the linear relationship of the parameters with the time constant is a good indicator for the performance of the asymmetric Gaussian as model function for the response function.

#163948 - $15.00 USD Received 1 Mar 2012; revised 16 Apr 2012; accepted 16 Apr 2012; published 10 May 2012

Total response

The convolution of the sample response function [Eq. (12)] with the lock-in-amplifier instrument response function [Eq. (13)] leads to the total response function

$$F(t,\tau) = \left(\alpha_{\mathrm{pr}} * R_{\mathrm{LIA}}\right)(t,\tau) = \int_{-\infty}^{\infty} \alpha_{\mathrm{pr}}(x,\tau) R_{\mathrm{LIA}}(x-t)\mathrm{d}x, \tag{15}$$

which is taken as fitting model for all experimental data from the polarimeter setup. With the help of Eq. (15) we can extract the parameters α_0, η, d_{pu}, and d_{pr} from experimental data.

Acknowledgments

The authors are grateful to Michael Knauer for steady-state optical rotation dispersion measurements and to Florian Langhojer for support and fruitful discussions during the early stage of this project. AS thanks the German National Academic Foundation (Studienstiftung des deutschen Volkes) for a scholarship. This publication was funded by the German Research Foundation (DFG) in the funding program Open Access Publishing. PN further acknowledges the DFG for financial support within the Emmy-Noether program.

#163948 - $15.00 USD Received 1 Mar 2012; revised 16 Apr 2012; accepted 16 Apr 2012; published 10 May 2012